and back portion of the airfoil is shown in Figs. 2b and 2c, respectively. The smooth transition of the grid from one type to another and the decency of the grid at sharp corners and between close surfaces are clearly shown, which indicate excellent compatibility and communication between the two grid strategies as controlled by a common background grid. The grid was generated using a Silicon Graphics IRIS 4D/210 VGX workstation. The code's performance is about 360 triangles/s on that workstation and 2350 triangles/s on a Cray Y-MP. The total turnaround time required for generating a grid around a complex geometry, including the setup time, is about 1 h.

To examine the fidelity of the grids generated with the present method, a turbulent viscous-flow computation was performed on the grid shown in Fig. 2. The flow solution was obtained with an available node-based, upwind flow solver[8] using the Baldwin-Barth turbulence model at a Mach number of 0.2, an angle of attack of 16.2 deg, and a Reynolds number of $9 \times 10^6$. Comparisons for surface pressure distributions and velocity profiles are shown in Figs. 3a and 3b, respectively. Excellent agreement with experimental data confirms the viability of the generated grid.

## Concluding Remarks

A new method of unstructured viscous grid generation has been introduced. The approach is conceptually simple but powerful, and capable of producing high-quality viscous unstructured grids for complex configurations with ease. Being based on a totally unstructured grid strategy, the method is fully automatic and flexible and, thus, alleviates the difficulties stemming from the structural limitations of the existing structured or semi-unstructured techniques. Because of an efficient grid-marching strategy and a simple front-detection algorithm, the method is highly efficient and operational on small workstations. The method is also self-sufficient for insertion of grid points in the boundary layer and beyond.

The method has been applied to two-dimensional problems with satisfactory results. The basic elements of the technique, however, have been primarily designed for its subsequent extension for generating three-dimensional highly stretched tetrahedral grids which is currently in progress. The full benefit of the method will be realized for generation of three-dimensional viscous grids where the complexity of the problem becomes excessive.

## References

[1]Mavriplis, D. J., "Euler and Navier-Stokes Computations for Two-Dimensional Geometries Using Unstructured Meshes," Inst. for Computer Applications in Science and Engineering, NASA Langley Research Center, Rept. 90-3, NASA CR-181977, Jan. 1990.

[2]Nakahashi, K., "Optimum Spacing Control of the Marching Grid Generation," AIAA Paper 91-0103, Jan. 1991.

[3]Kallinderis, Y., and Ward, S., "Prismatic Grid Generation with an Efficient Algebraic Method for Aircraft Configurations," AIAA Paper 92-2721, June 1992.

[4]Ward, S., and Kallinderis, Y., "Hybrid Prismatic/Tetrahedral Grid Generation for Complex 3-D Geometries," AIAA Paper 93-0669, Jan. 1993.

[5]Parikh, P., Pirzadeh, S., and Löhner, R., "A Package for 3-D Unstructured Grid Generation, Finite Element Flow Solution and Flow Field Visualization," NASA CR-182090, Sept. 1990.

[6]Pirzadeh, S., "Recent Progress in Unstructured Grid Generation," AIAA Paper 92-0445, Jan. 1992.

[7]Pirzadeh, S., "Structured Background Grids for Generation of Unstructured Grids by Advancing Front Method," AIAA Journal, Vol. 31, No. 2, 1993, pp. 257–265; also AIAA Paper 91-3233, Sept. 1991.

[8]Anderson, W. K., and Bonhaus, D. L., "An Implicit Upwind Algorithm for Computing Turbulent Flows on Unstructured Grids," Computers and Fluids, Vol. 23, No. 1, 1994, pp. 1–21.

# Influence of Impingement Edge Geometry on Cavity Flow Oscillations

J. C. F. Pereira* and J. M. M. Sousa†
*Instituto Superior Técnico, 1096 Lisbon, Portugal*

## Introduction

THERE is a variety of engineering flow applications and systems that can be modeled as single or as series of cavities, including slotted-wall wind and water tunnels, aircraft components, depressions in submarine and ship hulls, computer boards with closely spaced chip carriers, or even the gasdynamic laser cavities. Experimentally, it has been observed that the fluid flow in and near cavity-type geometries is unsteady, usually exhibiting large-amplitude oscillations of pressure and velocity. Although it is undeniable that the flow oscillations may be beneficial in certain cases (e.g., to enhance heat transfer rates), in most cases they are pernicious, causing structural vibration and noise, as well as increasing drag. Therefore attenuation of cavity oscillations is a relevant subject.

The experiments of Sarohia[1] for laminar axisymmetric flow have proved that the reported flow oscillations were not a result of resonance phenomena based on the interaction of the separated shear-layer deflection and internal cavity pressures. The mechanism that sustains the oscillations in such impinging flows was later investigated by Rockwell and Knisely.[2] In their work, they have shown that these flows are dominated by vortical structures that form upstream, in the vicinity of the separation edge, and impinge at the downstream edge of the cavity. The presence of this edge leads to an enhancement of the organization of the aforementioned shear layer. Moreover, the interaction between the vortical structures and the impingement corner was found to generate a feedback mechanism, sustaining markedly coherent fluctuations.[3,4] Hence, it is reasonable to expect that modifications of the downstream cavity edge geometry will give rise to important changes in the specific characteristics of cavity flow oscillations. Simple modifications may, from this standpoint, allow for the achievement of a major reduction in the oscillations amplitude.

The present experiments embrace visualization of the shear-layer flow past three different cavity edge geometries (sharp, nose-shape, and round), as well as detailed laser Doppler anemometry measurements of the time-averaged velocity flowfield and turbulent velocity characteristics. The information reported herein aims to characterize the influence of the impingement edge geometry on unsteady cavity flow and it is further used to assess the effectiveness of the modified configurations (nose-shape and round corners) in attenuating the flow oscillations.

## Experimental Procedure and Instrumentation

The experimental setup consisted of a cavity model formed on the floor of a water tunnel made of PERSPEX, 0.170 m in depth, 0.200 m in width, and 7 m in length. The water was drawn from a constant-head discharge tank and pumped, in a closed-circuit, into a pressurized tank, as described by Durão et al.[5] The cavity model spanned the test section by a combination of appropriate upstream and downstream plates, yielding a depth-to-cavity length ratio of $h/b = 0.5$ and a depth-to-width ratio of $h/w = 0.12$ for $h/H = 0.141$, where $H$ is the channel height. The incoming turbulent channel flow Reynolds number was $Re_H = 20,440$, the turbulence intensity at the channel centerline was approximately 4%, and the corresponding cavity flow was characterized by a Reynolds number, based on the cavity depth $h$ and channel centerline velocity $U_O$,
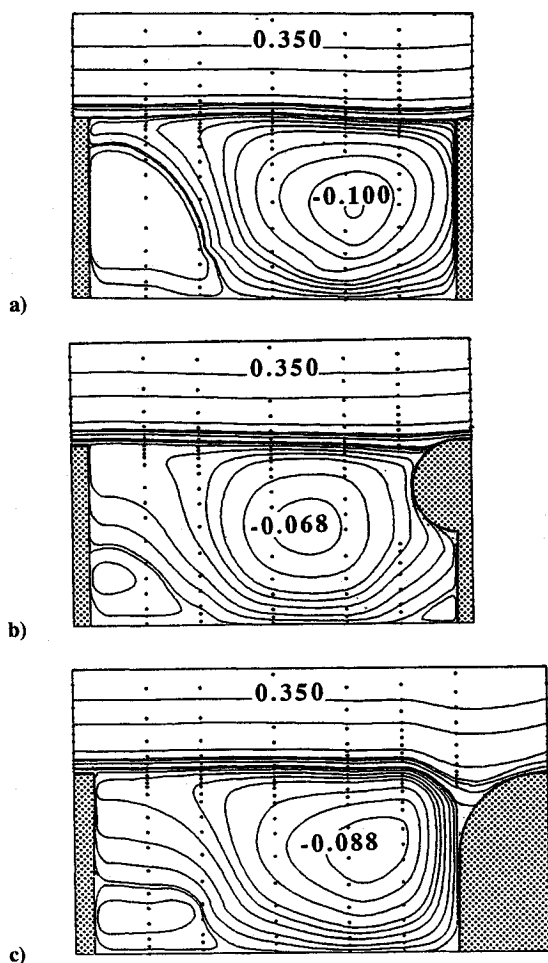
Fig. 1   Time-averaged flow streamlines (dots indicate measuring locations). Level values: –0.100, –0.088, –0.068, –0.052, –0.035, –0.026, –0.018, –0.008, –0.004, –0.001, 0.000, 0.002, 0.018, 0.028, 0.035, 0.068, 0.210, 0.350: a) sharp edge, b) nose-shape edge, and c) round edge.

$Re_h$ = 3360. Besides the standard rectangular cavity (sharp edges), two modified downstream cavity edges were employed: a nose-shape edge, consisting of a half-circle of radius $h/4$ added to the top half of the forward-facing step of the cavity; and a round edge, obtained by smoothing the sharp impingement edge in the shape of a quarter-circle of radius $h/2$.

To adequately visualize the separated shear-layer structures, a fluid tracer was utilized (a solution of Rhodamin 6 G particles). A laser light (Spectra-Physics 2540 Ar-Kr laser) from above illuminated the channel centerplane and video-recorded pictures were then taken, at right angles to the sheet of light, using a charge-coupled device camera. The images were later processed and digitized, allowing a frame-by-frame analysis, aiming to produce a detailed characterization of the impingement edge effect on the organization of the flow. A 15-mW (nominal) He-Ne laser (NEC GL G5600) was employed as laser source for the velocimeter, which was operated in the dual-beam forward-scatter mode with sensitivity to the flow direction provided by light-frequency shifting (0.2 MHz) from Bragg cells. The photomultiplier output signal was bandpass filtered and processed by a TSI 1980B frequency counter. Time-averaged velocities and turbulent velocity statistics were evaluated by ensemble averaging, calculated from 20,000 to 60,000 samples of the validated data read into a digital computer. It should be mentioned that the systematic errors due to nonturbulent Doppler broadening[6] were found to be negligibly small. Also, the random (statistical) errors[7] have never exceeded 1 and 3%, concerning the mean and variance values, respectively, by virtue of the large number of samples used to form the averages.

## Results and Discussion

The results presented in this section include flow visualization and detailed time-averaged and turbulent velocity characteristics, obtained in the centerline of vertical planes across the cavity. The Reynolds number was kept unchanged and equal to $Re_h$ = 3360. Figure 1 shows the time-averaged flow streamlines, corresponding to the investigated geometries, evaluated from the measured streamwise velocity component. The mean flow patterns reveal the dissimilitudes of the flow structures inside the cavity, depending upon the geometry of the downstream corner. One should note that the assumption of flow two-dimensionality was satisfactorily veri-
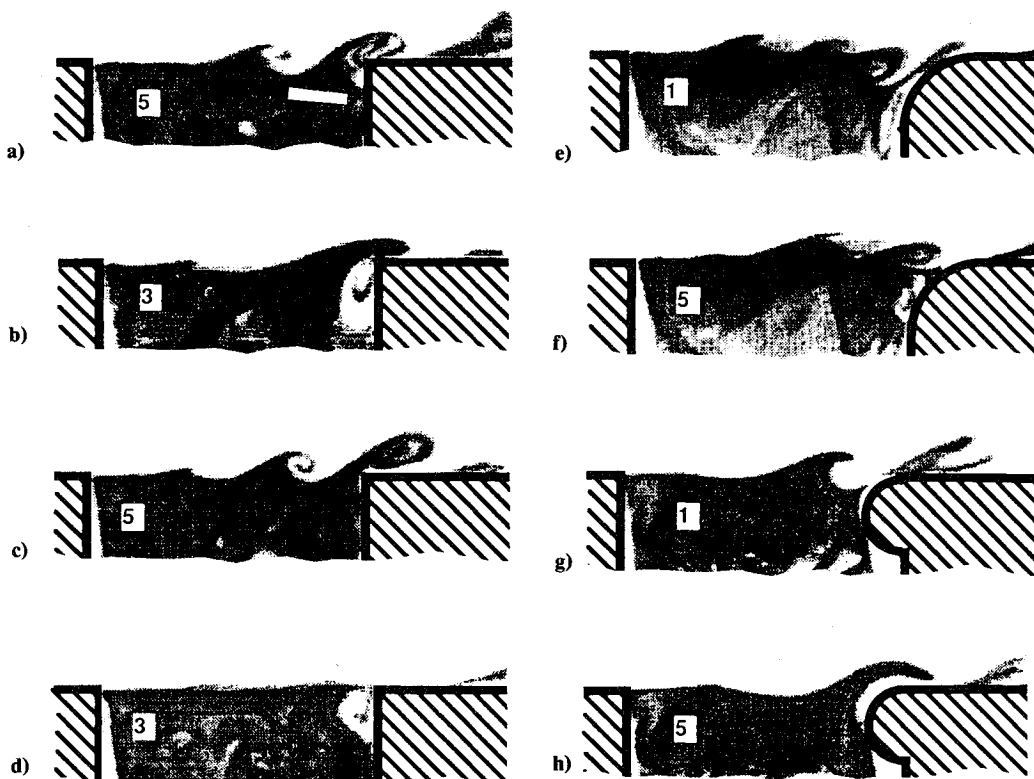


Fig. 2   Flow visualization of the separated shear layer, for different impingement cavity edges, showing the vortex-edge interaction.
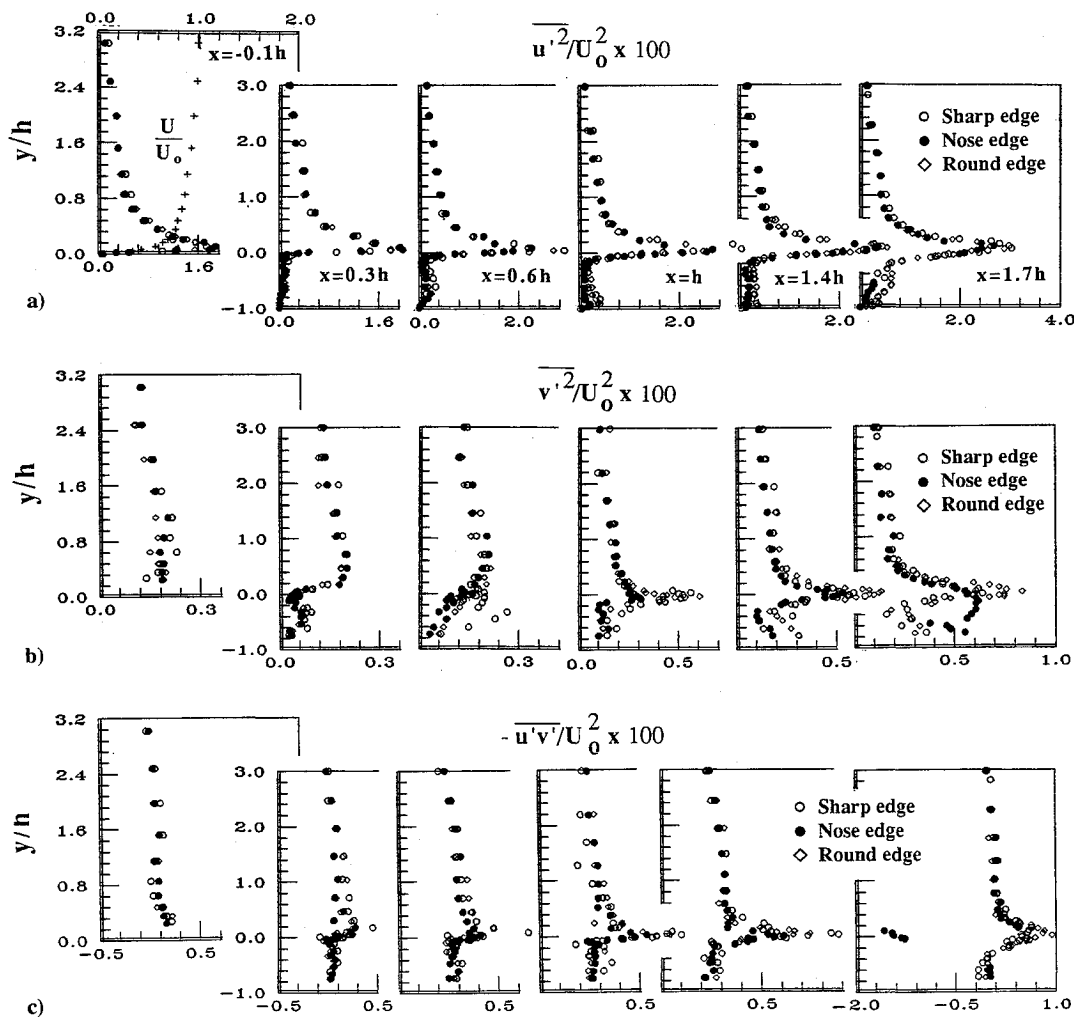
**Fig. 3    Turbulent velocity characteristics at various locations across the cavity: a)variance of streamwise velocity fluctuations, b) variance of vertical velocity fluctuations, and c) Reynolds shear stress.**

fied for the aforementioned moderate Reynolds number, through the comparison between the actual streamwise velocity profile and two others measured at spanwise locations $w/4$ and $3w/4$.

Close inspection of the mean streamlines presented in Fig. 1 leads to the observation that the nose-shape and round edge geometries, with particular emphasis to the latter, induce a more nearly perpendicular impingement of the stagnation streamline than the sharp edge geometry. As a consequence, the size of the primary eddy is larger. The maximum negative values of the nondimensional stream function inside the cavities are $-0.102$, $-0.070$, and $-0.096$, corresponding to Figs. 1a, 1b, and 1c, respectively. Thus, one may further conclude that the use of the round, and particularly of the nose, edge geometries implies a decrease in the drag force appertinent to the presence of the cavity, in comparison with the standard cavity geometry (sharp edge).

The unsteady nature of the flow is illustrated in Fig. 2, showing the possible fates which may occur as a typical shear-layer vortex approaches the cavity impingement edge. The snapshots suggest the presence of organized flow oscillations. This was confirmed by the spectral information extracted from velocity time series, measured in the shear-layer region past middle impingement length, which displayed a quasiperiodic behavior. The power spectra of the vertical velocity component indicated a dominant frequency of oscillation, corresponding to a Strouhal number $S_t = 1.1$ ($S_t = fb/U_O$, where $f$ is the dimensional frequency). A striking feature is that, despite the evident differences in the flow structure, the same dominant frequency was measured in the three cavity flows. The obtained Strouhal number is in excellent agreement with previously reported measurements,[8] for a standard rectangular cavity (sharp edge), corresponding to the designated second mode, the

most frequent mode for $b/h = 2$. The presence of the same dominant frequency in the shear layer, using the three different impingement edges denotes that, for the present geometries, the recirculating flowfield does not alter dramatically the inner shear-layer structure. However, in the following paragraphs, it will be demonstrated that the shape of this edge plays an important role in determining the extent of the upstream influence, which in turn is associated with the vorticity distribution of the incident vortex.

Figures 2a and 2b portray the most frequent events for the case of a sharp impingement edge, termed by Rockwell and Knisely[9] as "partial escape" and "partial clipping," respectively, where a part of the vortex is severed and swept downward. A less frequent event, described as "complete escape" of the vortex, can be observed in Fig. 2c. In this case, the vortex is not clipped and continues downstream retaining its integrity. Finally, Fig. 2d depicts the most unfrequent event, the "complete clipping" of the impinging shear-layer vortex, whereby the entire structure is swept downward. In contradistinction, when using the round impingement edge geometry, "complete clipping" is frequently observed (see the sequence formed by Figs. 2e and 2f), constituting the predominant event. It is associated with the large displacement of the impinging vortex core location, allowing the whole structure to be swept downward. The injection of fluid into the recirculation region then augments the amplitude of the flow oscillations. In the near region of the downstream corner, the flow is usually less organized than for the other investigated geometries, displaying an important three-dimensional character. As will be discussed at the end of this section, the present round corner geometry does not lead to an attenuation of the oscillations amplitude, although Ethembabaoglu[10] found a significant reduction of these oscilla-

tions using a similar edge. However, in his experiments, the edge was formed by a 1:5 ellipse instead of the one-quarter circle employed in the present investigation. Concerning the case of a nose-shape impingement corner geometry, the preferred event corresponds to "complete escape" of the approaching shear-layer vortex, as shown in the sequence of Figs. 2g and 2h. Moreover, the roll-up of the shear-layer vortical structures is generally incipient, implying that the arising vortices rarely achieve the maturity evidenced by those observed for the remaining geometries, hence facilitating a "complete escape."

The profiles of Reynolds normal and shear stresses are presented in Fig. 3, at different longitudinal stations in the cavity region. The time-averaged fluctuating flow characteristics are a result of random and periodic contributions that have not been decomposed in the present work. The development of the normal and shear stresses reveals a qualitatively similar distribution in the separated shear-layer region over the cavities, due to similar velocity fields and, hence, rates of strain. The magnitude of normal stresses increases very rapidly in the first cavity half. However, the variance of vertical fluctuating velocities displays much smaller peak values for the nose-shape edge geometry than for the remaining geometries. The results evince that the nose-shape geometry yields an effective reduction of the vertical oscillations amplitude. Based on flow visualization and time-averaged velocity characteristics, one can associate the ocurrence of vortex escape to a decrease in the maximum values of fluctuating velocities, while both partial and complete clipping contribute to the reinforcement of the vertical velocity fluctuations. Large differences in the time-averaged fluctuating velocity characteristics were measured inside the cavity mainly as a result of the different time-averaged flow structure.

## Conclusions

Flow visualization and laser Doppler measurements have provided detailed information about the effect of the impingement edge geometry on both instantaneous and time-averaged characteristics of a cavity flow displaying organized oscillations. The use of three different downstream cavity edge geometries (sharp, nose-shape, and round) did not alter the corresponding Strouhal number value, $S_t = 1.1$, despite the fact that the recirculating flowfield inside the cavity was markedly influenced by the downstream corner geometrical detail. Attenuation of the fluctuation peak magnitudes was presented for the nose-shape impingement edge. The flow visualization bears that this attenuation is a direct consequence of the most frequent escape of the separated shear-layer vortices approaching the impingement edge.

## References

[1] Sarohia, V., "Experimental Investigation of Oscillations in Flows Over Shallow Cavities," AIAA Journal, Vol. 15, No. 7, 1977, pp. 984–991.

[2] Rockwell, D., and Knisely, C., "The Organized Nature of Flow Impingement Upon a Corner," Journal of Fluid Mechanics, Vol. 93, Pt. 3, 1979, pp. 413–432.

[3] Knisely, C., and Rockwell, D., "Self-Sustained Low-Frequency Components in an Impinging Shear Layer," Journal of Fluid Mechanics, Vol. 116, March 1982, pp. 157–186.

[4] Rockwell, D., "Oscillations of Impinging Shear Layers," AIAA Journal, Vol. 21, No. 5, 1983, pp. 645–664.

[5] Durão, D. F. G., Heitor, M. V., and Pereira, J. C. F., "A Laser Anemometry Study of Separated Flow Over a Model Three-dimensional Hill," Applications of Laser Anemometry to Fluid Mechanics, edited by R. J. Adrian, T. Asanuma, D. F. G. Durão, F. Durst, and J. H. Whitelaw, Springer-Verlag, Berlin, 1989, pp. 93–118.

[6] Durst, F., Melling, A., and Whitelaw, J. H., Principles and Practice of Laser-Doppler Anemometry, 2nd. ed., Academic Press, New York, 1981, Chap. 7.

[7] Yanta, W. J., and Smith, R. A., "Measurements of Turbulent-Transport Properties with a Laser-Doppler Velocimeter," AIAA Paper 73-169, 1978.

[8] Rockwell, D., "Prediction of Oscillation Frequencies for Unstable Flow Past Cavities," ASME Journal of Fluids Engineering, Vol. 99, No. 2, 1977, pp. 294–300.

[9] Rockwell, D., and Knisely, C., "Vortex-Edge Interaction: Mechanisms for Generating Low Frequency Components," Physics of Fluids, Vol. 23, No. 2, 1980, pp. 239, 240.

[10] Ethembabaoglu, S., "On the Fluctuating Flow Characteristics in the Vicinity of Gate Slots," Div. of Hydraulics Engineering, Univ. of Trondheim, Norwegian Inst. of Technology, Norway, June 1973.

# Comparative Study of Higher Order Turbulence Models for Compressible Separated Flows

C. C. Chuang* and C. C. Chieng†
*National Tsing Hua University,
Hsinchu, Taiwan 30043, Republic of China*

## I. Introduction

ALTHOUGH turbulent separated flow has been the subject of many studies in the past few years, little of the reported research addressed high speed, as it related to the processes of separation, shear layer development, reattachment, and interaction of shock wave/separation. Predicting compressible turbulent separation is challenging both numerically and physically because the application of higher order turbulent closures requires solving highly coupled and nonlinear transport equations. Most studies use the algebraic turbulence models to eliminate the complexity of numerical and physical modeling. Recently, several investigations have incorporated a $k$-$\epsilon$ two-equation turbulence model when solving for transonic flows over bumps,[1,2] where the results showed an underestimation of shock-wave/boundary-layer interaction and a mismatch in the measured and computed shock location. An algebraic stress model (ASM) has also been successfully implemented and improves the predictions for the same problems.[2] Extensive experience in the incompressible environment suggests that second moment closure turbulence models are necessary for a satisfactory prediction of recirculating, curved flows.[3] Use of the second moment closure model sharply increases the difficulty in numerical stability arising from the stiff problem near the wall. Therefore, the solution algorithm is important in achieving convergence with high accuracy.

The objective of the present study was to examine the performance of Chien's low Reynolds number $k$-$\epsilon$ turbulence model,[4] ASM/$k$-$\epsilon$ two-layer model,[2] and Shima's near-wall Reynolds stress model[5] for predicting the transonic shock-induced separated flowfields over bump. Chien's $k$-$\epsilon$ model was chosen because of its simplicity, easy implementation, and stability when applied to complex flows. The inclusion of the high anisotropic effect of the turbulent stresses in the immediate vicinity of wall and the easy assessment of the empirical constants for the pressure-strain term are the reasons for choosing Shima's Reynolds stress model for this study.

## II. Physical and Mathematical Models

The governing equations used to describe the mean flow for this study are the time-dependent, mass-averaged, compressible Navier-Stokes equations. Depending on the two-equation $k$-$\epsilon$ model or Reynolds stress turbulence model used, the mean flow equations are augmented by additional transport equations of ($k$ and $\epsilon$) or ($\overline{u_i' u_j'}$ and $\epsilon$) where $k$, $\epsilon$ and $\overline{u_i' u_j'}$ are the turbulent kinetic energy, dissipation rate, and Reynolds stress components. The governing equation written in vector form in the ($\xi$, $\eta$) coordinate system can be expressed as

$$\partial_t (\hat{Q}) + \partial_\xi (\hat{E} - \hat{E}_v) + \partial_\eta (\hat{F} - \hat{F}_v) + j (\hat{H} - \hat{H}_v) = \hat{W} \qquad (1)$$